ACS NANO

www.acsnano.org

ARTICLE

# Deciphering the Role of PEGylation on the Lipid Nanoparticle-Mediated mRNA Delivery to the Liver

Menghua Gao, Jiafeng Zhong, Xinxin Liu, Yanjun Zhao, Dingcheng Zhu, Xiaohuo Shi, Xuehan Xu, Qin Zhou, Wenjing Xuan, Yue Zhang, Yaofeng Zhou,* and Jianjun Cheng*

Cite This: https://doi.org/10.1021/acsnano.4c09399

Read Online

ACCESS | Metrics & More | Article Recommendations | Supporting Information

**ABSTRACT:** **Organ- and cell-specific delivery of mRNA via modular lipid nanoparticles (LNPs) is promising in treating various diseases, but targeted cargo delivery is still very challenging. Most previous work focuses on screening ionizable and helper lipids to address the above issues. Here, we report the multifacial role of PEGylated lipids in manipulating LNP-mediated delivery of mRNA to the liver. We employed the typical excipients in LNP products, including DLin-MC3-DMA, DPSC, and cholesterol. Five types of PEGylated lipids were selected, and their molar ratio was fixed at 1.5% with a constant PEG molecular weight of 2000 Da. The architecture of steric lipids dramatically affected the in vitro gene transfection, in vivo blood clearance, liver deposition, and targeting of specific cells, all of which were closely linked to the de-PEGylation rate. The fast de-PEGylation resulted in short blood circulation and high accumulation in the liver. However, the ultrafast de-PEGylation enabled the deposition of more LNPs in Kupffer cells other than hepatocytes. Surprisingly, simply changing the terminal groups of PEGylated lipids from methoxyl to carboxyl or amine could dramatically increase the liver delivery of LNPs, which might be associated with the accelerated de-PEGylation rate and enhanced LNP−cell interaction. The current work highlights the importance of manipulating steric lipids in promoting mRNA delivery, offering an alternative approach for formulating and optimizing mRNA LNPs.**

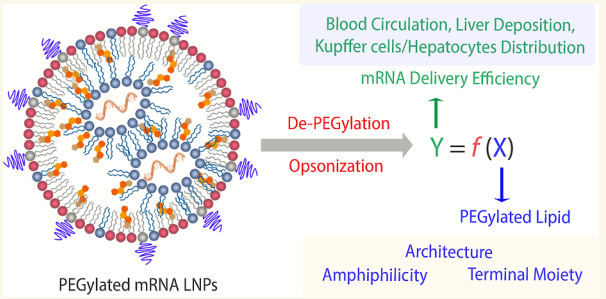


**KEYWORDS:** *nanomedicine, drug delivery, mRNA, PEGylation, lipid nanoparticles*

## INTRODUCTION

Messenger ribonucleic acid (mRNA) is a single-stranded sequence that carries genetic information from deoxyribonucleic acid (DNA) and serves as the template for protein synthesis.[1] In the past decade, mRNA has transformed into a particular class of therapeutic agents for prophylactically or therapeutically managing a myriad of diseases.[2−5] The stability and immunogenicity issues of mRNA necessitate the employment of modular delivery vectors for in vivo application.[6,7] The lipid nanoparticles (LNPs) are the most intensively investigated and clinically advanced nonvirus vehicles for mRNA delivery, and several LNP-based mRNA medicines have been successfully translated into the clinics.[8,9] A typical mRNA LNP consists of cholesterol, helper lipid, ionizable lipid, and steric lipid that usually contains hydrophilic poly(ethylene glycol) (PEG).[10] The ionizable lipid can electrostatically condense mRNA, forming reverse micelles within LNPs; upon endocytosis, the ionization of this lipid in acidic endosomes induces the formation of a nonbilayer hexagonal phase, triggering membrane damage and cargo release into the cytosol.[11] The PEGylated lipid forms a monolayer beyond the core of LNPs, ensuring steric stability and prolonged systemic circulation of LNPs.[12]

Despite the continuous effort to develop organ-specific mRNA LNPs, the liver is still the primary destination of mRNA nanomedicines because of the rich blood vessels and abundant macrophages (i.e., Kupffer cells) therein.[7,13−15] Previous work has focused on tailoring ionizable lipids to improve mRNA delivery via organ and cell targeting, but the role of PEGylated lipids in delivery efficiency is often neglected.[16−20] In fact, the PEGylated lipids affect the property

Received: July 13, 2024
Revised: November 29, 2024
Accepted: December 6, 2024

**Scheme 1. Schematic Illustration of the Influence of PEGylated Lipids on the Liver Delivery of mRNA LNPs**[a]

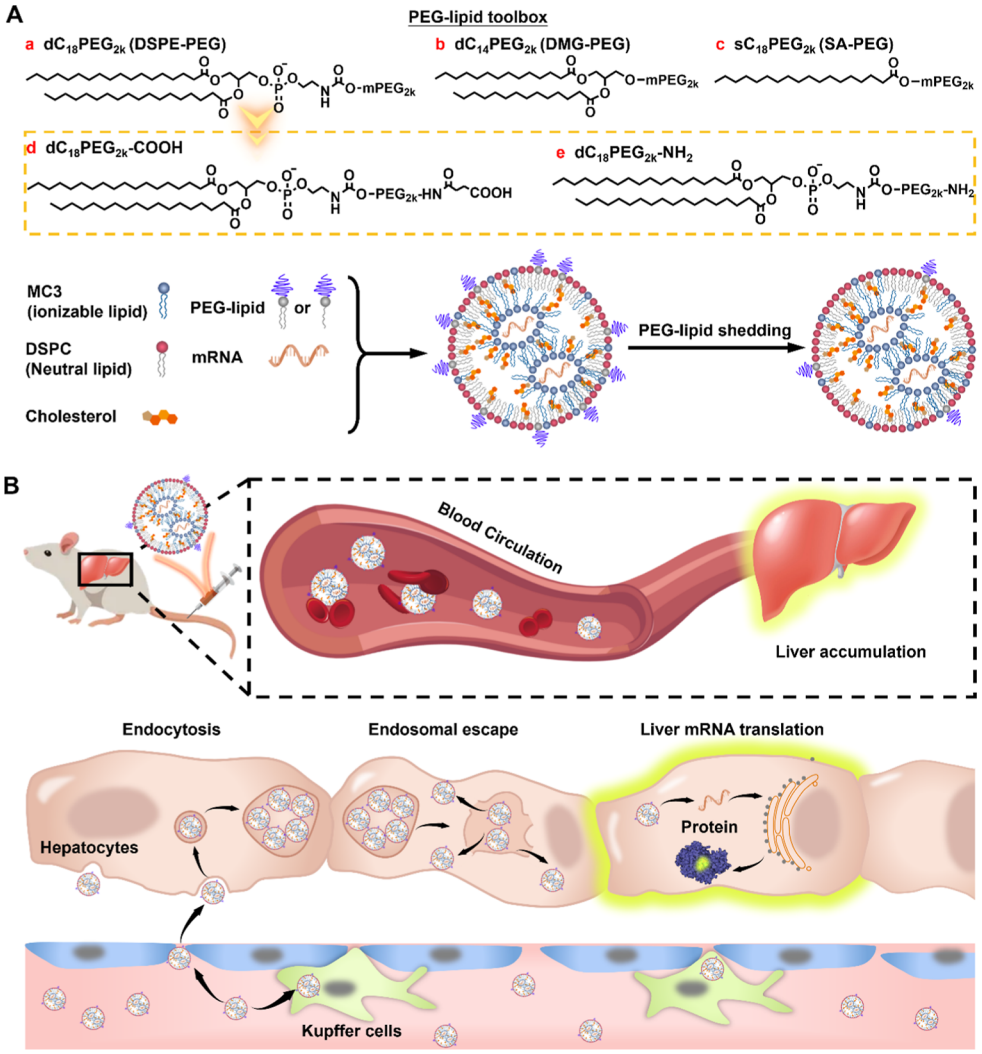


[a](A) The chemical structure of five selected PEGylated lipids and mRNA LNP components as well as the de-PEGylated LNPs. (B) PEGylated lipids determine the LNPs' systemic circulation, liver accumulation, endocytosis, endosomal escape, and mRNA translation in the cytosol.

and fate of LNPs from multiple aspects, including particle size, surface charge, stability against aggregation and serum protein adsorption, elimination by the mononuclear phagocyte system (MPS), pharmacokinetics, biodistribution, cellular uptake, and endosomal escape.[21] These behaviors are controlled mainly by the kinetics of de-PEGylation (i.e., shedding of PEG) that is determined by the architecture of PEGylated lipids.[8,22,23] Meanwhile, the LNP delivery is influenced by the terminal group of PEG, and tailored PEG terminal modification by fluorinated moieties could significantly enhance mRNA delivery via enhanced cellular uptake and endosomal escape.[24,25] However, the interplay among molecular weight (MW), topology, amphiphilicity, terminal group type, and charge of PEGylated lipids makes it challenging to optimize LNPs facilely.[19] Therefore, a comprehensive investigation into PEGylated lipids' role in mRNA delivery is urgent.

The aim of this work was to elucidate the correlation between PEGylated lipids and the delivery efficiency of mRNA LNPs, concerning de-PEGylation kinetics (i.e., PEG shedding rate), blood circulation, liver deposition, endocytosis, endosomal escape, and protein expression in vitro and in vivo (Scheme 1). [(6*Z*,9*Z*,28*Z*,31*Z*)-Heptatriaconta-6,9,28,31-tetraen-19-yl] 4-(dimethylamino)butanoate (abbreviated as DLin-MC3-DMA or MC3) was selected as the ionizable lipid that was widely utilized as one of the "gold standards" in mRNA LNP development.[26] Five types of PEGylated lipids were picked up based on the physicochemical property, including stearic acid-PEG conjugate (SA-PEG), 1,2-dimyristoyl-*rac*-glycero-3-methoxypolyethylene glycol (DMG-PEG), and PEGylated 1,2-dioleoyl-*sn*-glycero-3-phosphoethanolamine (DSPE-PEG) differing in terminal group (methoxyl, amine, or carboxyl). The PEG MW was fixed at 2000 Da for all PEGylated lipids. SA-PEG, DMG-PEG, and methoxyl DSPE-PEG were also abbreviated as $sC_{18}PEG_{2k}$, $dC_{14}PEG_{2k}$, and $dC_{18}PEG_{2k}$, respectively, based on the architecture of the aliphatic chain (single or double) and the length of the chain. Likewise, the amine- and carboxyl-terminated DSPE-PEG ions were named $dC_{18}PEG_{2k}$-$NH_2$ and $dC_{18}PEG_{2k}$-COOH.

## RESULTS

**Preparation and Characterization of PEGylated LNPs.** We focused on three LNPs (DSPE LNP, DMG LNP, and SA LNP) that shared the same ionizable lipid (MC3) and helper lipids (1,2-distearoyl-*sn*-glycero-3-phosphocholine/DSPC and


https://doi.org/10.1021/acsnano.4c09399
ACS Nano XXXX, XXX, XXX−XXX

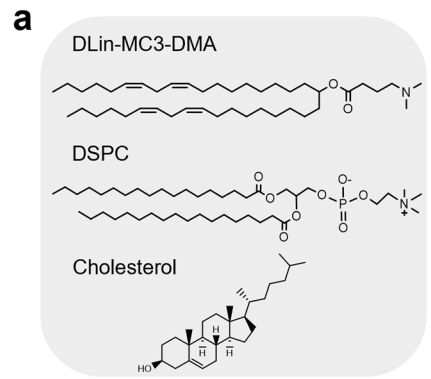


b

| Molar Ratio | DSPE LNP | | | DMG LNP | | | SA LNP | | |
|---|---|---|---|---|---|---|---|---|---|
| DLin-MC3-DMA | 50 | 50 | 50 | 50 | 50 | 50 | 50 | 50 | 50 |
| DSPC | 10 | 10 | 10 | 10 | 10 | 10 | 10 | 10 | 10 |
| Cholesterol | 38.5 | 38.5 | 38.5 | 38.5 | 38.5 | 38.5 | 38.5 | 38.5 | 38.5 |
| PEG-lipid | $dC_{18}PEG_{2k}$ | | | $dC_{14}PEG_{2k}$ | | | $sC_{18}PEG_{2k}$ | | |
| | 1.5 | 2.5 | 5 | 1.5 | 2.5 | 5 | 1.5 | 2.5 | 5 |

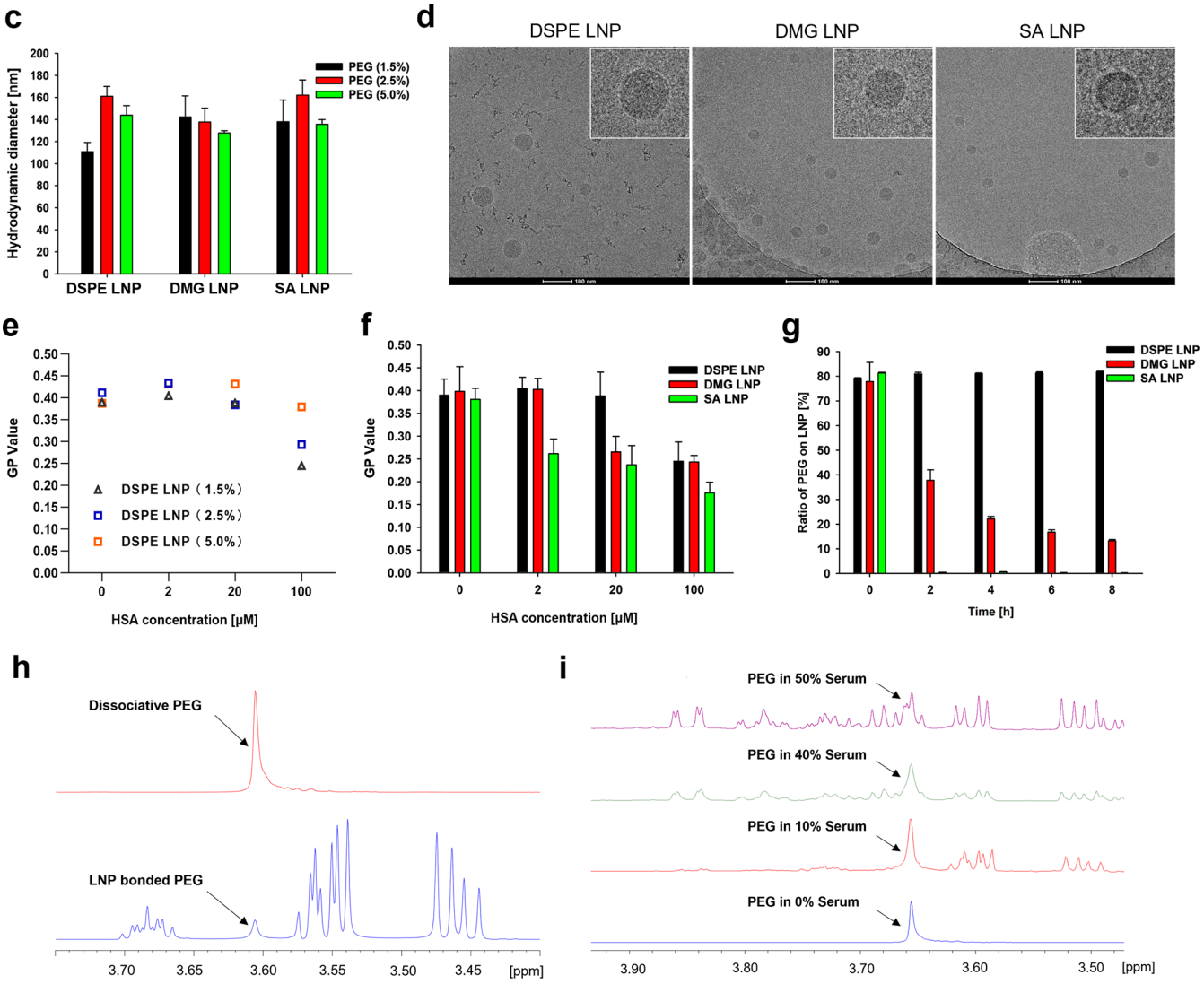


**Figure 1. Preparation and characterization of LNPs ($n$ = 3). (a) Chemical structures of ionizable lipid (DLin-MC3-DMA), helper lipid (DSPC), and cholesterol. (b) Formulation ingredient and the corresponding molar ratio in different LNPs. (c) Hydrodynamic diameters of LNPs with different surface PEG compactness measured by DLS. (d) Cryo-TEM images of DSPE LNP, DMG LNP, and SA LNP with a fixed PEG-lipid mole ratio at 1.5% (Scale bar: 100 nm). (e) HSA-induced shift of the GP value for three DSPE LNPs with different PEG levels (1.5%, 2.5%, and 5.0%). (f) Influence of HSA on the GP values of DSPE LNP, DMG LNP, and SA LNP with a constant 1.5% PEG for all LNPs. (g) Remaining PEG on the surface of three LNPs (1.5% PEG) post 40% MS incubation for 9 h measured and analyzed with PGSE-NMR. (h) Part of $^1$H NMR spectrum of PEG peak showing the difference between dissociative PEG and PEG that deposited onto the surface of DMG LNP. (i) Typical $^1$H NMR spectrum of PEG peak in DMG LNP, showing MS ratio-dependent signal and noise.**

cholesterol); the only difference was the PEGylated lipid (DSPE-PEG, DMG-PEG, and SA-PEG) (Figure 1a,b). Firefly luciferase (Fluc) mRNA was selected as the cargo for LNP encapsulation. The LNPs were prepared using the microfluidic technique, and three levels of PEGylated lipid content (1.5%, 2.5%, and 5.0%) were employed.[27,28] Irrespective of PEGylated


https://doi.org/10.1021/acsnano.4c09399
ACS Nano XXXX, XXX, XXX−XXX

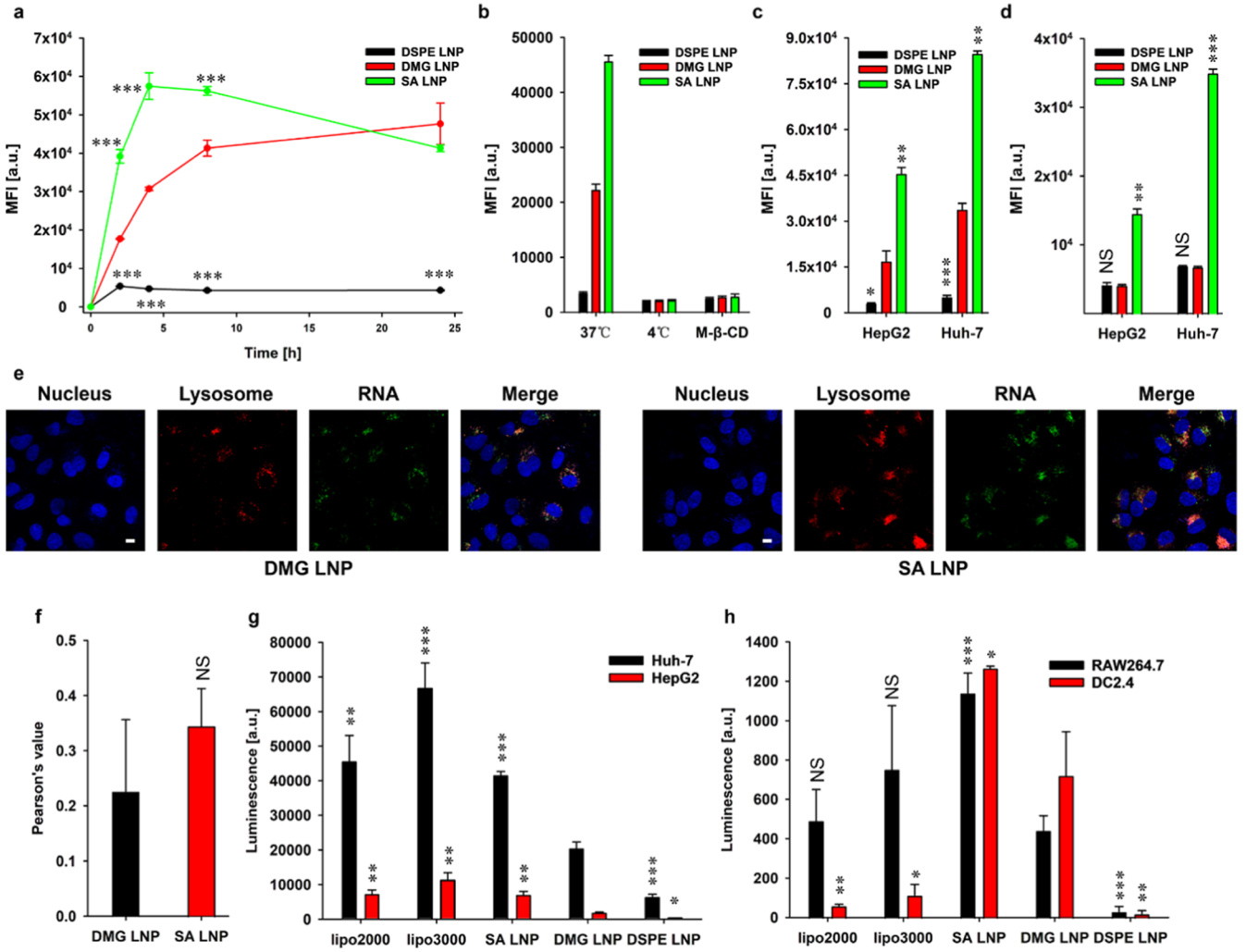


**Figure 2. Cellular uptake and endosomal escape of LNPs ($n$ = 3). (a) Flow cytometry analysis of MFI showing the kinetics of LNP uptake by Huh-7 cells. (b) Effect of temperature and methyl-$\beta$-cyclodextrin (m-$\beta$-CD) on the LNP uptake by Huh-7 cells at 2 h. Comparison of cellular internalization of LNPs at 4 h in the presence of (c) normal and (d) serum-free culture medium. (e) Confocal images of LNP-incubated Huh-7 cells, and the LNPs were loaded with fluorescence-labeled RNA (green), and the endosome/lysosome was imaged by LysoTracker (red). (f) Pearson's value-based colocalization analysis between LNPs and endosome/lysosome after 6 h incubation in Huh-7 cells. (g) In vitro Fluc mRNA expression in Huh-7 and HepG2 cells at 24 h with the aid of five vehicles, including lipo2000, lipo3000, DSPE LNP, DMG LNP, and SA LNP. (h) In vitro Fluc mRNA expression in RAW264.7 and DC2.4 cells at 24 h using the same vehicles. The statistical analysis was made with reference to DMG LNP unless otherwise stated. NS, no significant difference; *$p$ < 0.05, **$p$ < 0.01, and ***$p$ < 0.001.**

lipid type and concentration, all generated LNPs exhibited a hydrodynamic size of less than 200 nm with a narrow size distribution (Figure 1c and Table S1, Supporting Information). Increasing the PEGylated lipids ratio resulted in an irregular change of particle size for three LNPs despite the same MW of PEG (ca. 2000 Da) (Figure 1c). This was presumably due to the different amphiphilicity of these lipids that controlled the affinity between the PEGylated lipids and the lipophilic core of LNPs and hence the amount of PEG deposited onto the LNP surface. The three types of LNPs showed spherical morphology, as evidenced by the cryo-transmission electron microscopy analysis (Figure 1d). Besides, all LNPs exhibit a nearly neutral surface charge due to the presence of the hydrophilic steric PEG layer and the overall neutral charge of the DSPC component (Table S2, Supporting Information). The encapsulation efficiency (EE) of Fluc mRNA in LNPs was ca. 90% for all cases, indicating the high potency of MC3 in mRNA condensing (Table S3, Supporting Information).

Next, we employed Laurdan (6-dodecanoyl-2-(dimethylamino) naphthalene), a fluorescent probe sensitive to the membrane physical state and fluidity, to examine the steric stabilization effect of PEG.[29,30] Laurdan exhibits a phase order-dependent emission shift, allowing the quantification of membrane fluidity by ratiometrically determining the probe fluorescence intensity in two different channels, i.e., the generalized polarization (GP) value.[31] A high GP value usually indicates a low membrane fluidity and vice versa. Laurdan was first incubated with the different LNPs that were further challenged by human serum albumin (HSA), the major soluble constituent of human blood plasma, at different concentrations of up to 100 $\mu$M, followed by GP value calculation (Figure S1, Supporting Information). A significant shift of GP value signified a stronger interaction between LNPs and HSA, which was the case for the DSPE LNP containing 1.5% PEG other than other DSPE LNPs with a higher percentage of PEG (Figure 1e). At the same PEG level (1.5%), the HSA-induced particle instability indexed by GP shift ranked as follows: SA


https://doi.org/10.1021/acsnano.4c09399
ACS Nano XXXX, XXX, XXX−XXX

LNP > DMG LNP > DSPE LNP (Figure 1f), suggesting a higher degree of de-PEGylation for SA LNP in the presence of HSA. A similar trend has also been observed while all LNPs were incubated with 0.2% mouse serum (MS), respectively (Figure S2a,b, Supporting Information). In the following study, the PEG level was fixed at 1.5% for all LNPs unless otherwise stated.

To quantitatively assess the rate and extent of de-PEGylation of different LNPs, we employed the pulsed gradient spin echo nuclear magnetic resonance (PGSE-NMR) approach.[32] Such a method can determine the self-diffusion coefficient of selected components in solution and emerge as a robust method for studying nanoparticle microstructure.[33] The PEGylated lipid integrated with LNPs demonstrates a diffusion rate significantly slower than that of the free counterpart; the relative signals of these two populations can be quantified to reflect the kinetics of de-PEGylation (Figure 1h). The following experimental procedure continued with incubating all three LNPs with phosphate-buffered saline (PBS), 10% MS, and 40% MS, respectively. The de-PEGylation rate in PBS solution and 10% MS did not distinguish well for all these three LNPs, though the SA LNP showed about 15% PEG disassociation after incubating with 10% MS for 9 h (Figure S3b,c). While with 40% MS incubation, PEG was wholly removed from SA LNP within the first 20 min circle, indicating a very fast de-PEGylation speed caused by a high concentration of serum protein (Figure 1g and Figure S3a, Supporting Information). In contrast, de-PEGylation was not observed for DSPE LNP within 9 h, while there was ca. 40% and ca. 12% PEG remaining at 2 and 9 h regarding DMG LNP, respectively (Figure 1g and Figure S3a, Supporting Information). The results in Figure 1i show that the noise of PEG at this serum concentration has no significant effect on the detected PEG concentration, further confirming the reliability of the above conclusions. These LNPs' de-PEGylation discrepancies resulted from different affinities between PEG-lipid and LNP core. SA-PEG with the shortest and single aliphatic chain led to the unstable SA LNP, whereas DSPE LNP was the most stable one because of the long double fatty chains associated with PEG.

**Cellular Uptake and Endosomal Escape of PEGylated LNPs.** To explore the cellular behavior of LNPs, we encapsulated 5-carboxyfluorescein (FAM)-modified small interfering RNA (siRNA) in three types of LNPs. Similar physicochemical properties were observed for all LNPs in Table S4, irrespective of the cargo type (mRNA or siRNA). The internalization of LNPs by the human hepatocarcinoma cells (Huh-7) was examined by flow cytometry, and the RNA dose was fixed at 0.2 $\mu$g for LNPs (Figure 2a and Figure S4, Supporting Information). Irrespective of sampling time points, the extent of DSPE LNP uptake was significantly lower than DMG LNP ($p < 0.001$), which was because of the slow kinetics of de-PEGylation for DSPE LNP. Intriguingly, more SA LNP was taken up by Huh-7 cells than DMG LNP at 2 h, 4 h, and 8 h post-incubation ($p < 0.001$), which could be explained by the fast de-PEGylation for SA LNP. The de-PEGylation generally removes the hydrophilic PEG layer, favoring the transport of LNP across the lipid bilayer of cell membranes.[34] The triggered PEG shedding has been widely utilized for enhancing nanoparticle uptake.[35] Despite the difference in uptake rate, there was no significant difference in the extent of LNP uptake between SA LNP and DMG LNP at 24 h post-incubation ($p > 0.05$).

The endocytosis of all three LNPs was reduced at 4 °C compared to that at 37 °C, indicating an energy-dependent cellular uptake of particles (Figure 2b and Figure S5, Supporting Information). The presence of methyl-$\beta$-cyclodextrin (M-$\beta$-CD) significantly decreased the internalization of LNPs regardless of the de-PEGylation rate, suggesting the involvement of caveolin-mediated LNP uptake.[36,37] We also investigated the effect of the cell type on LNP uptake. The same trend of internalization was observed in another type of hepatocarcinoma cells (HepG2), but the extent of uptake in HepG2 cells was lower than in Huh-7 for all LNPs (Figure 2c). Cellular uptake experiments were carried out in a serum-free medium to determine the effect of protein adsorption on LNP internalization (Figure 2d and Figure S6, Supporting Information). Regardless of cell type, the uptake of DMG LNP at 4 h post-incubation was dramatically reduced to a level comparable to that of DSPE LNP ($p > 0.05$); the internalization of DSPE LNP was not affected by the removal of serum in the culture medium. These data suggest the critical role of protein adsorption in the uptake of DMG LNP.

The internalization of SA LNP in either HepG2 or Huh-7 cells was significantly higher than that in the other two counterparts, suggesting a highly complex uptake behavior of SA LNP in the absence of serum (Figure 2d and Figure S6, Supporting Information). Presumably, the rapid de-PEGylation for SA LNP may result in the adsorption of nonprotein molecules from the medium and/or the formation of large, aggregated particles due to hydrophobic interaction, which merits further investigation. Nevertheless, the internalization of SA LNP was dramatically reduced under serum-free conditions compared to those with serum. It is worth noting that PEG-free LNPs could not deliver nucleic acids into cells, indicating that the transient stabilization of LNP and gradual de-PEGylation were critical for gene delivery (Figure S7, Supporting Information).

Although in Huh-7 cells, the uptake of DMG LNP was lower than SA LNP after 6 h incubation, and there was no significant difference regarding the extent of endosomal escape indexed by Pearson's correlation coefficient ($p > 0.05$, Figure 2e,f). Pearson's correlation coefficient is a well-established index to assess the endosomal escape of nanoparticles.[38,39] The successful escape of LNPs from the acidic organelles is crucial for the cytosolic delivery of nucleic acids.[11] Considering the performance of uptake and endosomal escape, the degree of Fluc expression was ranked as follows: SA LNP > DMG LNP > DSPE LNP, which was valid in both types of hepatocarcinoma cells (Huh-7 and HepG2) (Figure 2g). Because the endosomal escape was similar for all lipid vehicles, the difference in Fluc expression primarily resulted from different uptake of LNPs. Due to the high charge density, Lipofectamine 2000 (abbreviated as lipo2000) and Lipofectamine 3000 (abbreviated as lipo3000), both commercial cationic liposome transfection reagents and commonly used as positive controls, were more potent than the above LNPs regarding mRNA translation. In all cases, the Fluc mRNA transfection was higher in Huh-7 cells than HepG2 cells, indicating cell-type-dependent mRNA delivery efficiency. The LNP-mediated Fluc mRNA transfection in macrophages (RAW264.7) and dendritic cells (DC2.4) was analogous to that in liver cells with the same ranking order (Figure 2h). However, the highly cationic lipo2000 and lipo3000 were not superior to LNPs in this case. Moreover, irrespective of vehicle type, the total amount of expressed Fluc in immune cells was


https://doi.org/10.1021/acsnano.4c09399
ACS Nano XXXX, XXX, XXX−XXX

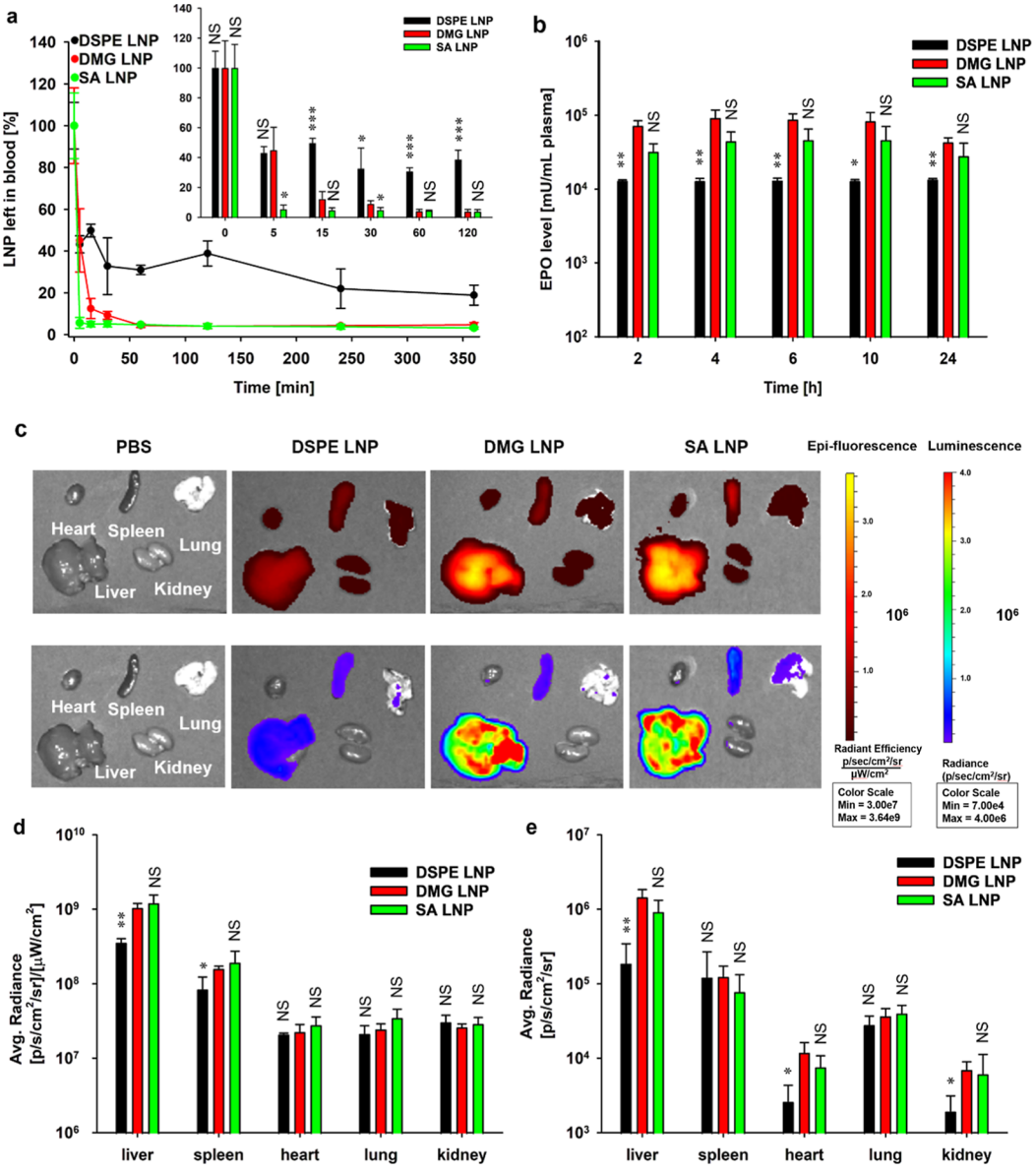


**Figure 3. Pharmacokinetics and biodistribution of three LNPs (DSPE LNP, DMG LNP, and SA LNP) in mice ($n$ = 3). (a) Remaining DiD-labeled EPO mRNA LNPs in blood circulation at predetermined time points post-intravenous (i.v.) injection with an insertion figure showing the data within the first 2 h. (b) Kinetic EPO expression in plasma of mice post-i.v. administration of EPO mRNA LNPs. (c) Ex vivo images of primary organs (heart, liver, spleen, lung, and kidney) showing the DiR fluorescence (top) and Fluc bioluminescence (bottom) of DiR-labeled Fluc mRNA LNPs, and the image was taken at 4 h post-i.v. administration. Statistical comparison of (d) DiR fluorescence and (e) Fluc bioluminescence in primary organs 4 h post-administration of DiR-labeled Fluc mRNA LNPs. The statistical analysis was made with reference to DMG LNP unless otherwise stated. NS, no significant difference; *$p$ < 0.05 and **$p$ < 0.01.**

much lower than that in liver cells, highlighting the difficulty of mRNA delivery to the immune cells.[40]

**Pharmacokinetics and Biodistribution of PEGylated LNPs.** The pharmacokinetics and biodistribution of nanomedicines determine the therapeutic efficacy and off-target effect.[41] In the current work, the EPO mRNA encoding human erythropoietin (EPO) protein was loaded into the three types of LNPs (i.e., DSPE LNP, DMG LNP, and SA LNP) to assess the LNP pharmacokinetics (Figure 3a). The LNPs were labeled with a fluorescent probe (DiD) for convenient signal collection. Regarding prolonged blood circulation, DSPE LNP was superior to DMG LNP and SA LNP, presumably due to the high affinity between DSPE-PEG and the lipids in the LNP core. Because of the rapid de-PEGylation, only a tiny amount of SA LNP remained in the circulation just 5 min after intravenous (i.v.) injection. DMG LNP was also rapidly eliminated, and there was no significant difference between the remaining DMG LNP and SA LNP in plasma until 15 min after i.v. administration. Such behavior of three LNPs was very consistent with their rate of de-PEGylation.

The plasma EPO level was employed as another indirect index of the pharmacokinetics and biodistribution of LNPs (Figure 3b). As a glycoprotein hormone, EPO primarily regulates human erythrocyte production.[42] Therefore, at the starting point of LNP administration (e.g., 0 h), the plasma EPO concentration was the same for all samples. In general, the EPO mRNA LNPs were taken up by liver cells during systemic circulation, and the EPO protein was then expressed


https://doi.org/10.1021/acsnano.4c09399
ACS Nano XXXX, XXX, XXX−XXX

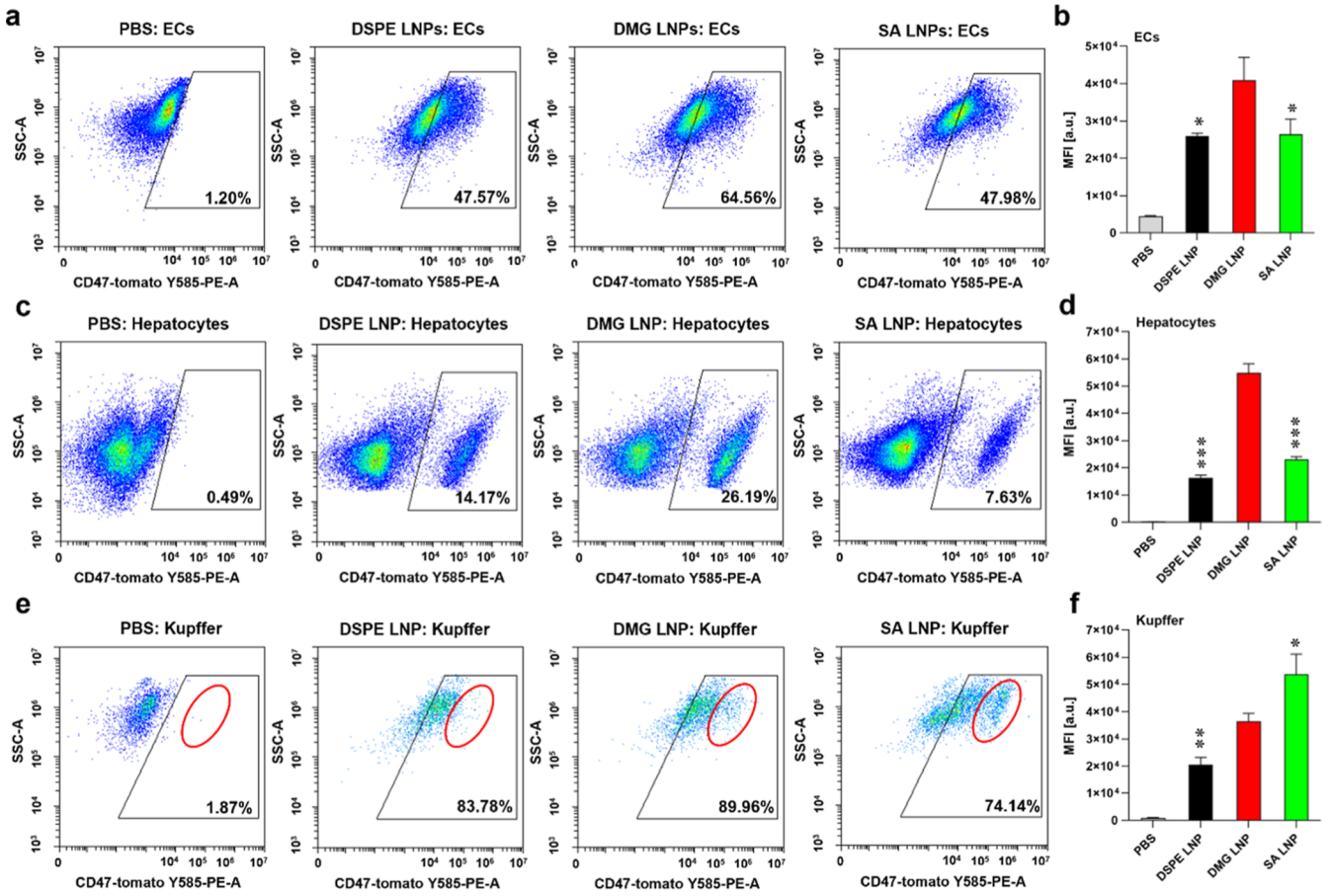


**Figure 4. Flow cytometry (FACS) analysis of LNP distribution in different liver cells identified and gated with specific antibody markers. Representative FACS images of tdTomato$^+$ cells in (a) endothelial cells (ECs), (c) hepatocyte cells, and (e) Kupffer cells in liver tissue of Ai14 mice 48 h post-treatment by PBS, DSPE LNP, DMG LNP, and SA LNP. The average tdTomato$^+$ percentage of each cell type for these treatments are presented in the right corner of the gating area (the statistical data are supplied in Figure S11, Supporting Information). The MFI in specific cells was shown in (b) ECs, (d) hepatocyte cells, and (f) Kupffer cells, respectively. The statistical analysis was made with reference to DMG LNP. *$p < 0.05$, **$p < 0.01$, and ***$p < 0.01$.**

therein before being released into the blood circulation. Due to the prolonged blood circulation of DSPE LNP, the extent of liver deposition would be reduced, resulting in the lowest EPO level in the plasma at all investigated time points. In contrast, DMG LNP and SA LNP showed a high level of EPO, indicating good liver distribution, cellular uptake, and mRNA transfection. This also suggests that the transient stabilization of LNPs and a suitable de-PEGylation rate are essential for the efficient delivery of mRNA to the liver.

Next, we encapsulated Fluc mRNA in the same type of LNPs that was further labeled with a DiR probe. DiR fluorescence and Fluc expression were employed as the indices for biodistribution assessment (Figure 3c and Figure S8, Supporting Information). At 4 h post-LNP administration, the accumulation of DSPE LNP in the liver and spleen was significantly lower compared to the other two counterparts, as evidenced by the fluorescence intensity of the DiR probe (Figure 3d). Likewise, with the Fluc bioluminescence as the index, a significantly weaker signal in the liver from the DSPE LNP group was observed, as was the deposition in the kidney and heart (Figure 3e). Irrespective of the index, there was no difference regarding the liver mRNA deposition of DMG LNP and SA LNP ($p > 0.05$), which may be explained by the rapid de-PEGylation, fast blood clearance, and liver accumulation for both particles.[43]

**Distribution of PEGylated LNPs in Different Liver Cells.** The Cre recombinase has been widely utilized to perform conditional mutagenesis of transgenes and insert DNA cassettes into eukaryotic chromosomes.[44] To assess the mRNA delivery distribution of different LNPs in various cells of the liver, we loaded Cre recombinase mRNA in three types of LNPs. These Cre mRNA LNPs were i.v. administered to Ai14 mice with a constant dose of 0.5 mg/kg. The cells of Ai14 mice possess a CAG-LoxP-STOP-LoxP-tdTomato construct, which causes the positive expression of the tdTomato fluorescence protein (tdTomato$^+$) upon the entry of Cre mRNA into the cytoplasm and its translation into the functional Cre protein. The Cre protein can edit the genome by excising the Stop cassette. At 48 h post-LNP injection, flow cytometry was employed to quantify the percentage of tdTomato$^+$ non-parenchymal cells and hepatocytes in the liver (Figure S9, Supporting Information).

Immunofluorescence staining revealed that DMG LNP and SA LNP-treated mice have higher tdTomato protein expression in macrophage cells than DSPE LNP-treated mice (Figure S10, Supporting Information). Such performance of the former two LNPs may be explained by the rapid de-PEGylation, followed by the sequestration by MPS that consists of a system of phagocytic cells, predominantly resident macrophages in the liver.[21] The FACS analysis proved the poor


https://doi.org/10.1021/acsnano.4c09399
ACS Nano XXXX, XXX, XXX−XXX

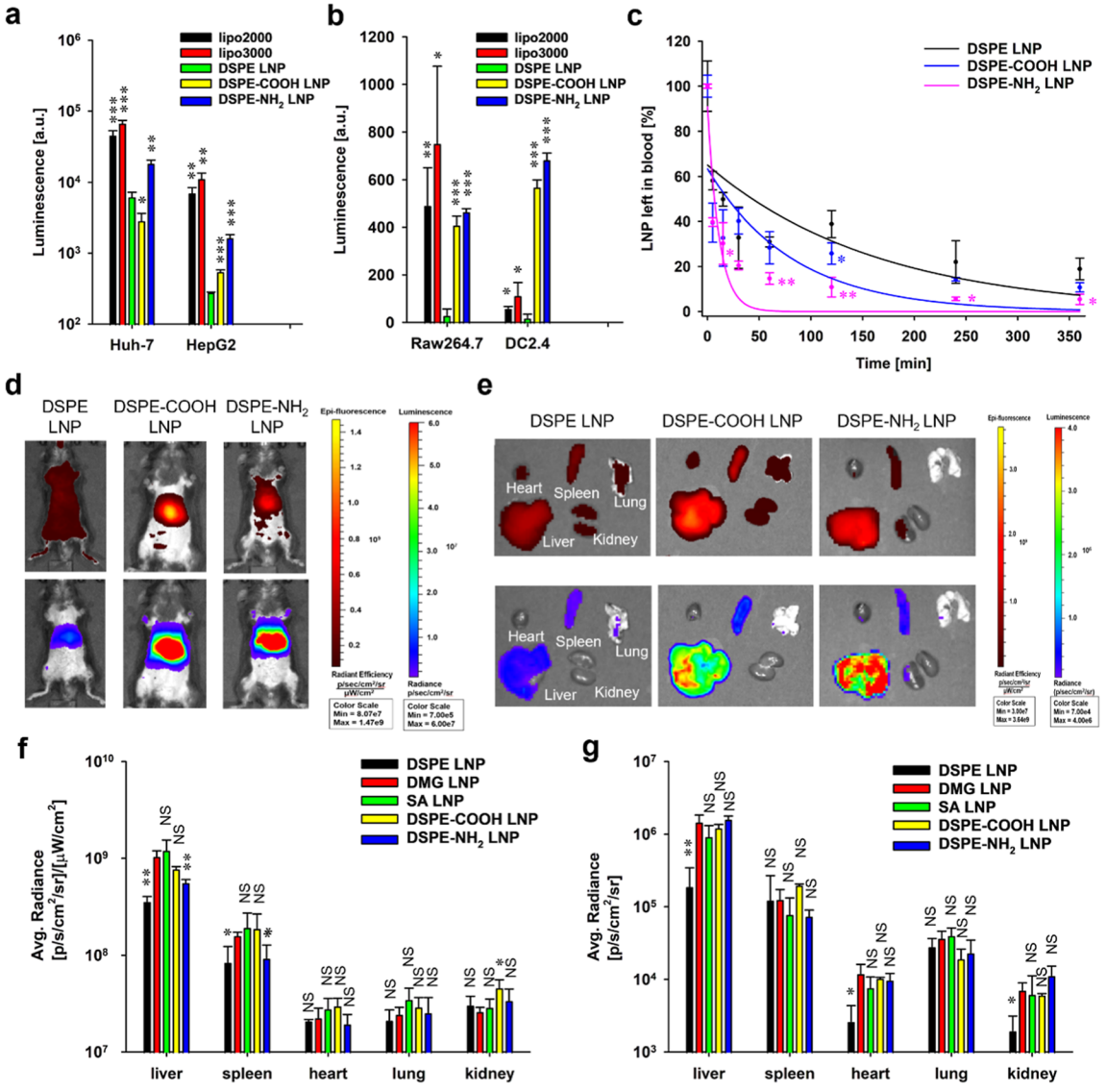


**Figure 5. Effect of PEG terminal group on the delivery efficiency of mRNA LNPs ($n$ = 3). (a) In vitro Fluc mRNA expression level in Huh-7 and HepG2 cells, and the mRNA vehicles were lipo2000, lipo3000, DSPE LNP, DSPE-COOH LNP, and DSPE-$NH_2$ LNP. (b) In vitro Fluc mRNA expression level in RAW264.7 and DC2.4 cells with the same vehicles. (c) Pharmacokinetics of DSPE LNP, DSPE-COOH LNP, and DSPE-$NH_2$ LNP. (d) In vivo distribution of LNPs at 4 h post-LNP administration with two indices, DiR fluorescence (top) and Fluc bioluminescence (bottom). (e) Ex vivo images of primary organs showing the DiR fluorescence (top) and Fluc bioluminescence (bottom) of DiR-labeled Fluc mRNA LNPs, and the image was taken at 4 h post-i.v. administration. The statistical analysis was made with reference to DSPE LNP. *$p$ < 0.05, **$p$ < 0.01, and ***$p$ < 0.001. Statistical analysis of (f) DiR fluorescence and (g) Fluc bioluminescence in major organs (liver, spleen, heart, lung, and kidney) for all LNPs were conducted. Mice were intravenously injected with different groups (PBS, DSPE LNP, DSPE-COOH LNP, DSPE-$NH_2$ LNP, DMG LNP, and SA LNP). All LNPs were labeled with DiR and loaded with Fluc mRNA. The statistical analysis was made with reference to the DMG LNP. NS, no significant difference; *$p$ < 0.05 and **$p$ < 0.01.**

mRNA delivery of DSPE LNP in all types of cells in the liver (Figure 4 and Figure S11, Supporting Information), which concurred well with the pharmacokinetics and biodistribution data of DSPE LNP (Figure 3). The prolonged systemic circulation of the DSPE LNP limited its liver accumulation. Though both DMG LNP and SA LNP exhibited similar nanoparticle distribution and potency in delivering mRNA cargos to the liver within 4−6 h (Figure 3), a higher tdTomato protein expression, programmed by Cre mRNA delivery in 48 h, was observed in Kupffer cells following SA LNP treatment (Figure 4 and Figure S11, Supporting Information). This may reflect the different cellular distributions immediately after systemic delivery of these two LNPs due to their similar levels of endosome escape efficiency (Figure 2e,f). Such a trend may be associated with the corresponding rate of de-PEGylation. The ultrafast shedding of PEG from SA LNP would induce more rapid MPS sequestration,[45,46] ultimately resulting in a significantly higher transfection of mRNA in Kupffer cells compared to DMG LNP ($p$ < 0.05). Conversely, protein expression in hepatocytes and endothelial cells following DMG LNP treatment was much higher than that of SA LNP treatment ($p$ < 0.001), likely due to a moderate de-PEGylation rate, which presumably avoids immediate MPS recognition and capture.

**Delivery Efficiency of LNPs Depends on the Terminal Group of PEG.** We further investigated the influence of


https://doi.org/10.1021/acsnano.4c09399
ACS Nano XXXX, XXX, XXX−XXX

terminal moieties of PEG on LNP potency regarding mRNA delivery. Due to the easy accessibility, we picked DSPE-PEG terminated with carboxyl and amine groups, i.e., DSPE-PEG-COOH and DSPE-PEG-$NH_2$. The MW of PEG was fixed at 2000 Da. The LNPs stabilized by the above PEGylated lipids were named DSPE-COOH LNP and DSPE-$NH_2$ LNP; the content of PEGylated lipids was the same at 1.5% for all LNPs (Figure S12, Supporting Information). These LNPs showed a high EE toward Fluc mRNA (ca. 90%), resulting in a hydrodynamic size of less than 150 nm with a narrow size distribution. The in vitro gene transfection in Huh-7 cells was ranked as follows: DSPE-$NH_2$ LNP > DSPE LNP > DSPE-COOH LNP (Figure 5a). However, the rank changed in the HepG2 cells: DSPE-$NH_2$ LNP > DSPE-COOH LNP > DSPE LNP. These data suggested the influence of particle surface group and cell type on gene delivery, and the different surface moieties may induce different cellular uptake levels of particles and then affect mRNA transfection efficiency. Irrespective of cell type, the positive control (lipo2000 and lipo3000) delivered more mRNA into the Huh-7 and HepG2 cells.

Regarding the immune cells, all three long-circulating LNPs and lipo2000/3000 showed a relatively low transfection efficiency compared to cancer cells (Figure 5b). This is because the immune cells are usually difficult to transfect by nonvirus vectors.[47] The Fluc luminescence in Raw264.7 cells and DC2.4 cells transfected by DSPE-$NH_2$ LNP and DSPE-COOH LNP was significantly larger than that by DSPE LNP ($p < 0.001$), highlighting the critical role of PEG terminal group in mediating gene delivery, which was often neglected. However, the Fluc signal was shallow in DC2.4 cells transfected by lipo2000/3000, which might be a consequence of lipofectamine's high charge density-induced cytotoxicity.[48] Intriguingly, the alternation in the PEG terminal group greatly affected the blood circulation of LNPs. DSPE-$NH_2$ LNP and DSPE-COOH LNP were more rapidly eliminated in the systemic circulation than DSPE LNP (Figure 5c), which may postulate to be linked to the different opsonization behaviors in circulation and further determines the remaining LNP in the blood. The accelerated PEG shedding behaviors for DSPE-$NH_2$ LNP and DSPE-COOH LNP were also proved by the in vitro PGSE-NMR measurements in Figure S13, Supporting Information, which showed ca. 50% PEG disassociation within 2 h, compared with DSPE LNP without terminal group modification.

The expedited blood circulation of DSPE-$NH_2$ LNP and DSPE-COOH LNP corresponded to increased liver accumulation, as evidenced by the intensity of both DiR fluorescence and Fluc bioluminescence (Figure 5d,e). We further compared the Fluc mRNA delivery efficiency of all LNPs employed in the current work (Figure 5f,g and Figure S14, Supporting Information). Surprisingly, DSPE-$NH_2$ LNP, DSPE-COOH LNP, and SA LNP showed a similar level of Fluc mRNA in the liver compared to the DMG LNP, though there was a little discrepancy when the DiR fluorescence intensity was utilized for quantification. To further explain the enhanced mRNA delivery by DSPE-$NH_2$ LNP and DSPE-COOH LNP, we performed the cellular mRNA delivery distribution using the tdTomato reporter Ai14 mice as in the above procedure. As shown in Figure S15, Supporting Information, the significant increase in mRNA delivery efficiency for these two LNPs with amine and carboxyl group modification is both found in hepatocyte cells according to the percentage of $tdTomato^+$ cells and the mean fluorescence intensity (MFI) of tdTomato protein, while no obvious change was found for endothelial cells and Kupffer cells. This type of in vivo behavior of these two LNPs is quite different from SA LNP, though the terminal group has accelerated the blood clearance rate. These results suggest that DSPE-COOH LNP and DSPE-$NH_2$ LNP are much more like the behavior of DSPE LNP over SA LNP, except for faster clearance and higher liver accumulation than the unmodified one. Combined with the in vitro cell transfection results and the in vivo blood clearance curve in Figure 5a–c, the enhanced liver mRNA delivery by DSPE-COOH LNP and DSPE-$NH_2$ LNP than the original DSPE LNP is caused by a series process containing deshielding in circulation, improved liver accumulation, and enhanced LNP–cell interaction. Difference in the detailed mechanism of in vivo transport and transfection process between the ultrafast de-PEGylation of SA LNP and the moderate de-PEGylation of DSPE-COOH LNP and DSPE-$NH_2$ LNP is still not clear. It may be speculated that all these could be explained by the LNP opsonization, MPS sequestration, and protein corona formation that was controlled by the de-PEGylation rate and PEG terminal moieties. However, the detailed mechanism necessitates the proteomics analysis, and it may be carefully studied and discussed in our future work.

## CONCLUSIONS

The current work comprehensively investigated how the PEGylated lipid affects the LNPs' potency regarding mRNA delivery to the liver. The architecture of PEG-lipid determines the affinity between the steric lipid and LNPs and hence the rate and extent of de-PEGylation in a biological environment. Intriguingly, ultrafast de-PEGylation of LNP can lead to increased liver mRNA delivery in Kupffer cells, liver-resident macrophages. Moreover, we also found that the increased liver delivery of mRNA could be achieved by simply manipulating the PEG terminal moieties (e.g., carboxyl and amine groups), accompanied with accelerated de-PEGylation rate, faster blood clearance, and enhanced nanoparticle–cell interaction. The mechanism of the different de-PEGylation behavior, the extent of MPS sequestration, the adsorption of plasma protein corona onto the LNPs, and eventually the liver deposition of LNPs still need further proteomic analysis and in vivo study. Overall, the discovery in this work highlights the complicated role of PEG in modulating the efficiency of LNPs in delivering mRNA to the liver and specific cells.

PEG-lipid construction and ionizable lipid engineering are pivotal strategies for enhancing mRNA delivery. PEG-lipid is crucial for maintaining particle stability, preventing rapid LNP clearance by MPS, and modulating the pharmacokinetics and biodistribution of LNPs. Ionizable lipids are essential for LNP performance, specifically in mRNA condensation, endosomal escape, and cytosolic cargo release. Future research should focus on optimizing the structure of PEG-lipid and ionizable lipids including MW, $pK_a$, and architecture. The interplay between PEG-lipid and ionizable lipid engineering should also be explored to elucidate the impact of excipient structure on LNP delivery performance, including PEG shedding, protein adsorption, organ and cell targeting, and immune response. Notably, nonliver delivery of mRNA by LNPs remains a significant challenge that warrants further fundamental investigation. Additionally, the biocompatibility, immunogenicity, and safety of these materials must be considered. Besides, anti-PEG IgG was commonly detected after SARS-CoV-2 vaccination, which is associated with systemic


https://doi.org/10.1021/acsnano.4c09399
ACS Nano XXXX, XXX, XXX–XXX

reactogenicity and may lead to the rapid complement opsonization of other PEGylated medicines.[49] Further study has reported that PEG shedding kinetics may alter the specific anti-PEG antibody production level.[50] Overall, our work implies the significant value of balancing LNP circulation and clearance behavior by manipulating PEG-lipid architecture during the rational design of the LNP-mRNA system.

## METHODS

**Materials.** DLin-MC3-DMA (MC3), 1,2-distearoyl-*sn*-glycero-3-phosphocholine (DSPC), cholesterol, and all PEG-lipids (including DMG (1,2-dimyristoyl-*rac*-glycero)-PEG2k, DSPE (1,2-distearoyl-*sn*-glycero-3-phosphoethanolamine)-PEG2k, DSPE-PEG2k-COOH/$NH_2$, and SA (stearic acid)-PEG2k) were purchased from AVT (Shanghai) Pharmaceutical Tech Co., Ltd. and Nanosoft polymers. EZ Cap FLuc mRNA (5-moUTP), EZ Cap EPO mRNA ($\psi$UTP), and *D*-luciferin (potassium salt) were purchased from APExBIO Technology LLC. Abs Cap Cre mRNA (5-moUTP) was purchased from Univ Biotech Co., Ltd. FAM (5-carboxyfluorescein)-labeled and unlabeled negative control (N.C.) siRNA was bought from GenePharm. Quant-iT RiboGreen RNA Assay Kit (R11490), Lipofectamine 2000 and 3000 (lipo2000 and lipo3000), 1,1′-dioctadecyl-3,3,3′,3′-tetramethylindodi-carbocyanine, 4-chlorobenzenesulfonate salt (DiD), and 1,1′-dioctadecyl-3,3,3′,3′-tetramethylindotricarbocyanine iodide (DiR) were purchased from ThermoFisher Scientific. Laurdan was purchased from Aladdin. Albumin from human serum was purchased from Sigma-Aldrich. MS was purchased from BioDee. ONE-Glo Luciferase assay system (E6120) was purchased from Promega. Antibodies including Allophycocyanin (APC) antimouse CD31, fluorescein isothiocyanate (FITC) antimouse CD45.2, and PE/Cy7 antimouse CD68 were purchased from BioLegend. Human EPO enzyme-linked immunosorbent assay (ELISA) kit was also bought from BioLegend (#442907). Antifade mounting medium with 4′,6-diamidino-2-phenylindole (DAPI) was from Beyotime Bio. $\alpha$-Smooth muscle actin ($\alpha$-SMA, ab124964) and hepatocyte nuclear factor 4 alpha (Hnf4$\alpha$, ab181604) were from Abcam (ab124964). F4/80 (no. 70076) was from Cell Signaling Technology. m-$\beta$-CD (methyl-$\beta$-cyclodextrin) was bought from Macklin.

**Animals.** Wild-type C57BL/6 mice, aged 6−8 weeks, were obtained from the Laboratory Animal Resources Center of Westlake University. LSL (loxP-STOP-loxP) tdTomato mice (Ai14), aged 4−8 weeks, were purchased from Cyagen Biosciences. The experimental protocols were reviewed and approved by the Institutional Animal Care and Use Committee (IACUC) at the School of Life Sciences, Westlake University (AP#21-051). All animal experiments were conducted by following the guidelines for the care and use of laboratory animals.

**Preparation of LNP by Microfluidic Mixing.** RNA-loaded LNPs were prepared using the ethanol dilution method with a microfluidic device (Micro&Nano Biologics).[51] Briefly, lipids were dissolved in ethanol in a mole ratio of 50:38.5:10:1.5 for MC3, cholesterol, DSPC, and PEG-lipid, respectively. The total concentration of the lipid mixture was 5 mM. The RNA was dissolved in 10 mM citrate buffer at pH 4.3. The lipids in ethanol and the RNA in citrate buffer were mixed in a microfluidic mixing chip at a flow rate of 12 mL/min, with a 1:3 ratio of the organic phase to the aqueous phase. The nitrogen: phosphate (N:P) ratio between the ionizable lipid (MC3) and RNA was maintained at 6 throughout the study. The resulting nanoparticles were then dialyzed against 1 × PBS buffer at pH 7.4 for 4 to 6 h at 4 °C using Pur-A-Lyzer Midi Dialysis kits (MWCO: 3.5 kDa, Sigma-Aldrich). For LNPs containing different types and ratios of PEG-lipids, the formulation manufacturing process was the same as that described above.

**LNP Characterization.** The hydrodynamic size and zeta potential of LNPs were characterized by using a dynamic light scattering (DLS) analyzer (BI-200SM, Brookhaven Instruments). Prior to analysis, LNPs were diluted with PBS or water to determine their size and zeta potential. To assess the RNA EE, the Quant-iT RiboGreen RNA assay kit was used in accordance with the manufacturer's instructions. Total RNA was determined by incubating LNPs with a 0.4% Triton X-100 solution at ambient temperature for 10 min. The fluorescence ($E_x/E_m$: 480/520 nm) of free and total RNA was measured using a BioTek Synergy H1microplate reader. Cryogenic-transmission electron microscopy (Cryo-TEM) was employed to analyze the size and morphology of the LNPs. LNP samples were concentrated using an ultrafiltration tube (MWCO: 3.5 kDa, Millipore) until the final lipid concentration reached approximately 14 mg/mL. The concentrated sample was then applied to a glow-discharged Carbon 300 mesh copper TEM grid (Electron Microscopy Sciences), blotted for 3−4 s with filter paper, and rapidly immersed in liquid ethane. Cryo-TEM image acquisition was conducted using a Glacios CRYO-EM001 (Thermo Fisher) high-resolution transmission electron microscope at an accelerating voltage of 200 kV, utilizing Ceta and Falcon cameras (Belliveau, 2012 #35).

**LNP−Protein Interaction Analysis.** The membrane fluidity of the LNP, affected by the interaction with surface proteins, was evaluated using the GP value of the polarity-sensitive fluorescent probe, Laurdan. Laurdan was dissolved as a 2.5 mM stock solution in dimethyl sulfoxide (DMSO). The LNP was diluted in PBS to a final lipid content of approximately 1 mM, and Laurdan was added to achieve a final concentration of 2.5 $\mu$M. The mixture was then incubated at 37 °C for 1 h, after which the Laurdan fluorescence was measured using a photoluminescence spectrometer (FLS1000, Edinburgh instruments) with an excitation wavelength of 375 nm.

To further investigate the interaction between the nanoparticle and proteins, LNPs labeled with Laurdan were mixed with three different concentrations of HSA, or MS, and the Laurdan fluorescence was immediately measured. The final concentrations of HSA used were 100 (high), 20 (medium), and 2 $\mu$M (low), respectively. The Laurdan fluorescence intensity spectra were scanned every 2 min from 400 nm to 550 nm for 10 min. Finally, all the spectra were compared to analyze the kinetics of the LNP surface−protein interaction.

**De-PEGylation Kinetics Measurement by PGSE NMR.** The shedding kinetics of surface PEG-lipids from LNPs were investigated using pulsed gradient spin echo (PGSE) nuclear magnetic resonance (NMR).[52] The underlying principle is that the diffusion of PEG on the LNP surface is constrained, resulting in a lower diffusion coefficient. However, once PEG is detached, the diffusion of PEG is significantly accelerated, leading to an increase in the diffusion coefficient. The main experimental procedure was as follows: 200 $\mu$L of LNPs loaded with nontargeting control (N.C.) siRNA (PEG-lipid concentration of 0.8 mg/mL), 250 $\mu$L of serum from male C57BL/6 mice, and 50 $\mu$L of deuterated water ($D_2O$) were mixed and transferred to a 5 mm NMR tube. The mixture was immediately subjected to detection using $^1$H PGSE NMR on a Bruker BioSpin (AVANCE NEO) 600 MHz NMR spectrometer. The detection parameters were optimized: a pulse gradient ranging from 5% to 96% in 16 steps, a diffusion time of 200 ms, a diffusion gradient increment of 10 ms, a relaxation time of 1 s, and an acquisition time of 4 s. The experiments were initiated at zero hour, and each cycle lasted approximately 20 min, with continuous monitoring for ca. 8−10 h. The NMR data obtained at the starting point reflected the degree of PEG detachment when LNPs were mixed with MS. The diffusion coefficients of PEG on the LNP surface, the diffusion coefficients of free PEG, and the signal intensities of the PEG peaks at each time point were separately calculated. The calculations followed the published equation.[32]

**Cell Uptake.** Huh-7 cells were cultured in Dulbecco's modified Eagle's medium (DMEM) supplemented with 10% fetal bovine serum (FBS) and 1% penicillin/streptomycin and maintained in a humidified incubator at 37 °C with 5% $CO_2$. For the cell uptake kinetic assay, Huh-7 cells were seeded in 24-well plates at a density of 40,000 cells per well and allowed to grow for 24 h before LNP treatment. All LNPs were prepared using nontargeting control small interfering RNA (N.C. siRNA) labeled with FAM. At various time points, the cells were collected, washed with PBS, and analyzed using flow cytometry (CytoFLEX, Beckman). The excitation wavelength was set at 490 nm, and emission wavelengths at 513 nm were used to


https://doi.org/10.1021/acsnano.4c09399
ACS Nano XXXX, XXX, XXX−XXX

detect the FAM fluorescence. Data analysis was performed by using FlowJo software.

To determine the endocytosis pathway by which LNPs were internalized, Huh-7 cells were initially treated with 10 mM m-$\beta$-CD (methyl-$\beta$-cyclodextrin) for 30 min at 37 °C. Then, the cells were washed and incubated with LNP-containing fresh medium. Subsequently, the cells were incubated for another 2 h at 37 °C before being collected for flow cytometry analysis. In parallel experiments, Huh-7 cells were separately incubated at 37 °C and 4 °C for 30 min. Fresh LNP-containing medium was added, and the cells were further incubated at 37 °C and 4 °C for 2 h. All cell samples were collected and analyzed simultaneously. Data analysis was performed using FlowJo software.

For the lysosome colocalization assay, Huh-7 cells were seeded in confocal culture dishes at a density of 100,000 cells and incubated overnight to allow for cell adherence. After the medium was replaced with fresh medium, LNPs containing FAM-labeled siRNA were added to each well and incubated for 6 h. Subsequently, the medium was replaced, and 75 nM lysosomal dye LysoTracker Red DND-99 (Thermo) was added. After 30 min, two drops of NucBlue Live ReadyProbes (Invitrogen) were added for nuclear staining, and the cells were further incubated for 15 min. The cells were washed three times and imaged by using a confocal Zeiss LSM980 microscope. Pearson's value indicating the colocalization level of FAM-siRNA and LysoTracker Red DND-99 fluorescence was conducted and analyzed using the plugin Coloc 2 in the Fiji (ImageJ) software. The value ranges from −1 to +1; +1 indicates a positive linear correlation, and −1 signifies a negative linear correlation.

**In Vitro Fluc mRNA Transfection Assay.** The transfection efficiency was assessed by using Fluc mRNA as a reporter gene. Two types of hepatic tumor cells (HepG2 and Huh-7) and two types of immune cells (RAW 264.7 and DC2.4), in a logarithmic growth phase, were seeded at an appropriate density in 96-well white-bottom plates (Bioland). Following overnight incubation, different LNP formulations containing 50 ng of Fluc mRNA were added to each well. After 24 h, the culture medium was removed, and ONE-Glo substrate (Promega, E6120) was employed. The substrate was completely dissolved and maintained at ambient temperature. Subsequently, the plate was shaken for 3 min using a plate shaker, and the bioluminescence intensity was measured. As positive controls, commercial transfection reagents lipo2000 and lipo3000 were used. Each sample was tested in quadruplicate wells.

**Pharmacokinetics of LNPs.** Pharmacokinetic studies were conducted with male C57BL/6 mice, aged 6−8 weeks. DSPE LNP, DMG LNP, and SA LNP containing EPO mRNA were administered to the mice via tail vein injection at a dosage of 0.5 mg/kg. All LNPs were labeled with a DiD dye, constituting 0.5% of the total lipid molar concentration. Each group consisted of three mice. Blood samples of approximately 50 $\mu$L were collected from the mouse orbital sinus at various time intervals, including 5 min, 15 min, 30 min, 1 h, 2 h, 4 h, 6 h, 10 h, and 24 h after intravenous injection. The collected blood sample was thoroughly mixed, and then 24 $\mu$L of the sample was lysed with 1% sodium dodecyl sulfate (SDS). Subsequently, the lysed sample was transferred to black 96-well plates, and the fluorescence intensity of DiD was measured ($E_x/E_m$: 640 nm/670 nm). The remaining plasma samples were centrifugated at 10,000$g$ for 10 min, and the resulting supernatant was collected for EPO expression measurement. An ELISA kit (Biolegend, #442907) was utilized for this purpose, and the serum samples were diluted (2000×).

**Biodistribution of LNPs.** The in vivo distribution and transfection studies utilized male C57BL/6 mice aged 6−8 weeks. Various LNPs containing 1.0% DiR (molar ratio) were administered to the mice via the tail vein at a dose of 0.15 mg/kg of mRNA. All LNPs loaded FLuc mRNA as the reporter gene, and each experimental group consisted of 3 mice ($n$ = 3). Following 4 h incubation, the mice were intraperitoneally injected with 200 $\mu$L of $D$-luciferin (15 mg/mL). The DiR fluorescence ($E_x/E_m$: 754 nm/778 nm) was immediately detected using a PerkinElmer IVIS Spectrum imaging system (PE Spectrum). The bioluminescence signal in the mice was continuously monitored for 15 min. The mice were euthanized, and the major organs (i.e., heart, liver, spleen, lung, and kidney) were dissected and imaged to assess further the distribution of particles and the luciferase activity in various organs. The imaging signals were then analyzed using the PerkinElmer software, Living image, and the signal intensity was quantified by selecting the region of interest (ROI).

**Distribution of LNPs in Different Cells of the Liver.** The distribution of LNPs in different liver cells was investigated in male Rosa-LSL-tdTomato reporter gene (Ai14) mice aged 6−8 weeks. Each mouse was administered various LNP formulations containing Cre mRNA via the tail vein, facilitating the expression of the tdTomato fluorescent protein. The injection dose was 0.5 mg/kg; each group consisted of three mice. After 48 h, the mice were anesthetized, and the liver was washed with HBSS buffer (Hanks' balanced salt solution) until they appeared tan. Subsequently, the liver tissue was minced and incubated in a digestion solution (composed of 5 mg/mL collagenase IV, 0.1 mg/mL DNase I, and 3 mM $CaCl_2$) with agitation at 37 °C for 30 min. The digested cells were then passed through a 70 $\mu$m cell strainer. The collected filtrate was treated with red blood cell lysis buffer on ice until the cells became colorless. Afterward, the cells were stained with specific antibodies according to the manufacturer's instructions for 15 min at ambient temperature. The antibodies used to identify specific liver cell types were as follows: APC-labeled antimouse CD31 (102409, Biolegend) for endothelial cells, FITC-labeled antimouse CD45.2 (109805, Biolegend) for leukocytes, and PE/Cy7-labeled antimouse CD68 (137015, Biolegend) for macrophages. Flow cytometry was employed to identify and analyze specific cell populations. PBS-treated mice were employed as the control to establish gates for the tdTomato-positive populations. A portion of the liver tissue was fixed in a 4% paraformaldehyde solution, stored in the dark at 4 °C, and used for immunofluorescence staining and imaging. The fixed tissue was embedded in paraffin, sectioned, and subjected to antibody staining for different liver cell markers, including DAPI for nuclear staining, $\alpha$-SMA for endothelial cell staining, Hnf4$\alpha$ for hepatocyte staining, and F4/80 for macrophage staining. After being stained, the tissue sections were observed under a microscope and photographed for comparison.

**Statistical Analysis.** The data were reported as the mean ± standard deviation (SD). All data were checked for normality (Kolmogorov−Smirnov test) and homogeneity of variances (Levene's test). The normally distributed data was analyzed by one-way analysis of variance (ANOVA) or Student's $t$-test. Other data were analyzed by the nonparametric Kruskal−Wallis and Mann−Whitney tests. Statistical significance was defined as a $p$-value less than 0.05. *$p$ < 0.05, **$p$ < 0.01, and ***$p$ < 0.001. All statistical tests and graphical representations were conducted using GraphPad Prism 9.

## ASSOCIATED CONTENT

### Supporting Information

The Supporting Information is available free of charge at https://pubs.acs.org/doi/10.1021/acsnano.4c09399.

Details of LNP characterization of size distribution, zeta potential, and EE; emission spectra of Laurdan-labeled LNPs in serum; PGSE NMR results of PEG dissociation in PBS and 10% MS; flow cytometry analysis results of LNP uptake; IVIS observation images of DiR fluorescence and Fluc bioluminescence; gating strategies and tdTomato$^+$ cells of different types of liver cells by flow cytometry analysis; immunofluorescence images of tdTomato$^+$ macrophages in liver; physicochemical characterization; PGSE NMR results of PEG dissociation; and IVIS images of biodistribution and tdTomato$^+$ cells of different types of liver cells by flow cytometry analysis of DSPE LNP, DSPE-COOH LNP, and DSPE-$NH_2$ LNP (PDF)



https://doi.org/10.1021/acsnano.4c09399
ACS Nano XXXX, XXX, XXX−XXX

## AUTHOR INFORMATION


### Corresponding Authors

**Jianjun Cheng** − *School of Engineering and Research Center for Industries of the Future, Westlake University, Hangzhou 310030 Zhejiang, China; Institute of Advanced Technology, Westlake Institute for Advanced Study, Hangzhou 310024 Zhejiang, China;* orcid.org/0000-0003-2561-9291; Email: chengjianjun@westlake.edu.cn

**Yaofeng Zhou** − *School of Engineering, Westlake University, Hangzhou 310030 Zhejiang, China; Institute of Advanced Technology, Westlake Institute for Advanced Study, Hangzhou 310024 Zhejiang, China*; Email: zhouyaofeng@westlake.edu.cn

### Authors

**Menghua Gao** − *School of Engineering, Westlake University, Hangzhou 310030 Zhejiang, China; Institute of Advanced Technology, Westlake Institute for Advanced Study, Hangzhou 310024 Zhejiang, China*

**Jiafeng Zhong** − *School of Engineering, Westlake University, Hangzhou 310030 Zhejiang, China*

**Xinxin Liu** − *School of Engineering, Westlake University, Hangzhou 310030 Zhejiang, China*

**Yanjun Zhao** − *Tianjin Key Laboratory for Modern Drug Delivery & High Efficiency, School of Pharmaceutical Science & Technology, Faculty of Medicine, Tianjin University, Tianjin 300072, China*

**Dingcheng Zhu** − *College of Life and Environmental Sciences, Hangzhou Normal University, Hangzhou 310036 Zhejiang, China;* orcid.org/0000-0002-5636-4976

**Xiaohuo Shi** − *Instrumentation and Service Center for Molecular Sciences, Westlake University, Hangzhou 310030, China*

**Xuehan Xu** − *School of Engineering, Westlake University, Hangzhou 310030 Zhejiang, China*

**Qin Zhou** − *School of Engineering, Westlake University, Hangzhou 310030 Zhejiang, China; Institute of Advanced Technology, Westlake Institute for Advanced Study, Hangzhou 310024 Zhejiang, China*

**Wenjing Xuan** − *School of Engineering, Westlake University, Hangzhou 310030 Zhejiang, China; Institute of Advanced Technology, Westlake Institute for Advanced Study, Hangzhou 310024 Zhejiang, China*

**Yue Zhang** − *School of Engineering, Westlake University, Hangzhou 310030 Zhejiang, China*

Complete contact information is available at: https://pubs.acs.org/10.1021/acsnano.4c09399


### Author Contributions

M.H.G., Y.F.Z., Y.J.Z., Y.Z. and J.J.C. conceived, designed, supervised this research, and drafted the manuscript. M.H.G., J.F.Z., and X.X.L. performed the experiments and provided technical advice. Y.F.Z., D.C.Z., X.H.S., X.H.X., Q.Z., and W.J.X. provided intellectual input and helped perform the experiments. All authors approved the final version of the manuscript.

### Notes

The authors declare no competing financial interest.

## ACKNOWLEDGMENTS

This work was supported by Pioneer and "Leading Goose" R&D Program of Zhejiang (2024SDXHDX0004), the National Natural Science Foundation of China (52233015 for J.C. and 22407112 for M.G.), and China Postdoctoral Science Foundation (2024T170813). We acknowledges the support from the New Cornerstone Investigator Program, New Cornerstone Science Foundation.

## REFERENCES


(1) Wang, J.; Zhu, H.; Gan, J.; Liang, G.; Li, L.; Zhao, Y. Engineered MRNA Delivery Systems for Biomedical Applications. *Adv. Mater.* **2024**, *36* (15), No. e2308029.

(2) Huang, X.; Kong, N.; Zhang, X.; Cao, Y.; Langer, R.; Tao, W. The Landscape of MRNA Nanomedicine. *Nat. Med.* **2022**, *28* (11), 2273−2287.

(3) Barbier, A. J.; Jiang, A. Y.; Zhang, P.; Wooster, R.; Anderson, D. G. The Clinical Progress of MRNA Vaccines and Immunotherapies. *Nat. Biotechnol.* **2022**, *40* (6), 840−854.

(4) Shen, G.; Liu, J.; Yang, H.; Xie, N.; Yang, Y. mRNA Therapies: Pioneering a New Era in Rare Genetic Disease Treatment. *J. Controlled Release* **2024**, *369*, 696−721.

(5) Liu, X.; Huang, P.; Yang, R.; Deng, H. mRNA Cancer Vaccines: Construction and Boosting Strategies. *ACS Nano* **2023**, *17* (20), 19550−19580.

(6) Xiao, Y.; Tang, Z.; Huang, X.; Chen, W.; Zhou, J.; Liu, H.; Liu, C.; Kong, N.; Tao, W. Emerging MRNA Technologies: Delivery Strategies and Biomedical Applications. *Chem. Soc. Rev.* **2022**, *51* (10), 3828−3845.

(7) Dilliard, S. A.; Siegwart, D. J. Passive, Active and Endogenous Organ-Targeted Lipid and Polymer Nanoparticles for Delivery of Genetic Drugs. *Nat. Rev. Mater.* **2023**, *8* (4), 282−300.

(8) Hou, X.; Zaks, T.; Langer, R.; Dong, Y. Lipid Nanoparticles for MRNA Delivery. *Nat. Rev. Mater.* **2021**, *6* (12), 1078−1094.

(9) Paunovska, K.; Loughrey, D.; Dahlman, J. E. Drug Delivery Systems for RNA Therapeutics. *Nat. Rev. Genet.* **2022**, *23* (5), 265−280.

(10) Li, B.; Raji, I. O.; Gordon, A. G. R.; Sun, L.; Raimondo, T. M.; Oladimeji, F. A.; Jiang, A. Y.; Varley, A.; Langer, R. S.; Anderson, D. G. Accelerating Ionizable Lipid Discovery for MRNA Delivery Using Machine Learning and Combinatorial Chemistry. *Nat. Mater.* **2024**, *23* (7), 1002−1008.

(11) Chatterjee, S.; Kon, E.; Sharma, P.; Peer, D. Endosomal Escape: A Bottleneck for LNP-Mediated Therapeutics. *Proc. Natl. Acad. Sci. U.S.A.* **2024**, *121* (11), No. e2307800120.

(12) Wang, M. M.; Wappelhorst, C. N.; Jensen, E. L.; Chi, Y.-C. T.; Rouse, J. C.; Zou, Q. Elucidation of Lipid Nanoparticle Surface Structure in MRNA Vaccines. *Sci. Rep.* **2023**, *13* (1), 16744.

(13) Dilliard, S. A.; Cheng, Q.; Siegwart, D. J. On the Mechanism of Tissue-Specific MRNA Delivery by Selective Organ Targeting Nanoparticles. *Proc. Natl. Acad. Sci. U.S.A.* **2021**, *118* (52), No. e2109256118.

(14) Wang, X.; Liu, S.; Sun, Y.; Yu, X.; Lee, S. M.; Cheng, Q.; Wei, T.; Gong, J.; Robinson, J.; Zhang, D.; Lian, X.; Basak, P.; Siegwart, D. J. Preparation of Selective Organ-Targeting (SORT) Lipid Nanoparticles (LNPs) Using Multiple Technical Methods for Tissue-Specific mRNA Delivery. *Nat. Protoc.* **2023**, *18* (1), 265−291.

(15) Loughrey, D.; Dahlman, J. E. Non-Liver MRNA Delivery. *Acc. Chem. Res.* **2022**, *55* (1), 13−23.

(16) Kon, E.; Ad-El, N.; Hazan-Halevy, I.; Stotsky-Oterin, L.; Peer, D. Targeting Cancer with MRNA-Lipid Nanoparticles: Key Considerations and Future Prospects. *Nat. Rev. Clin. Oncol.* **2023**, *20* (11), 739−754.

(17) Zong, Y.; Lin, Y.; Wei, T.; Cheng, Q. Lipid Nanoparticle (LNP) Enables MRNA Delivery for Cancer Therapy. *Adv. Mater.* **2023**, *35* (51), No. e2303261.

(18) Melamed, J. R.; Hajj, K. A.; Chaudhary, N.; Strelkova, D.; Arral, M. L.; Pardi, N.; Alameh, M.-G.; Miller, J. B.; Farbiak, L.; Siegwart, D. J.; Weissman, D.; Whitehead, K. A. Lipid Nanoparticle Chemistry Determines How Nucleoside Base Modifications Alter mRNA Delivery. *J. Controlled Release* **2022**, *341*, 206−214.

(19) Eygeris, Y.; Gupta, M.; Kim, J.; Sahay, G. Chemistry of Lipid Nanoparticles for RNA Delivery. *Acc. Chem. Res.* **2022**, *55* (1), 2−12.
(20) Huang, P.; Deng, H.; Wang, C.; Zhou, Y.; Chen, X. Cellular Trafficking of Nanotechnology-Mediated MRNA Delivery. *Adv. Mater.* **2024**, *36* (13), No. e2307822.
(21) Blanco, E.; Shen, H.; Ferrari, M. Principles of Nanoparticle Design for Overcoming Biological Barriers to Drug Delivery. *Nat. Biotechnol.* **2015**, *33* (9), 941−951.
(22) Zhu, X.; Tao, W.; Liu, D.; Wu, J.; Guo, Z.; Ji, X.; Bharwani, Z.; Zhao, L.; Zhao, X.; Farokhzad, O. C.; Shi, J. Surface De-PEGylation Controls Nanoparticle-Mediated SiRNA Delivery In Vitro and In Vivo. *Theranostics* **2017**, *7* (7), 1990−2002.
(23) Ryals, R. C.; Patel, S.; Acosta, C.; McKinney, M.; Pennesi, M. E.; Sahay, G. The Effects of PEGylation on LNP Based MRNA Delivery to the Eye. *PLoS One* **2020**, *15* (10), No. e0241006.
(24) Zhang, H.; Meng, C.; Yi, X.; Han, J.; Wang, J.; Liu, F.; Ling, Q.; Li, H.; Gu, Z. Fluorinated Lipid Nanoparticles for Enhancing mRNA Delivery Efficiency. *ACS Nano* **2024**, *18* (11), 7825−7836.
(25) Yu, X.; Li, H.; Dong, C.; Qi, S.; Yang, K.; Bai, B.; Peng, K.; Buljan, M.; Lin, X.; Liu, Z.; Yu, G. Poly(Ethyl Ethylene Phosphate): Overcoming the "Polyethylene Glycol Dilemma" for Cancer Immunotherapy and MRNA Vaccination. *ACS Nano* **2023**, *17* (23), 23814−23828.
(26) Han, X.; Zhang, H.; Butowska, K.; Swingle, K. L.; Alameh, M.-G.; Weissman, D.; Mitchell, M. J. An Ionizable Lipid Toolbox for RNA Delivery. *Nat. Commun.* **2021**, *12* (1), 7233.
(27) Shepherd, S. J.; Warzecha, C. C.; Yadavali, S.; El-Mayta, R.; Alameh, M.-G.; Wang, L.; Weissman, D.; Wilson, J. M.; Issadore, D.; Mitchell, M. J. Scalable MRNA and SiRNA Lipid Nanoparticle Production Using a Parallelized Microfluidic Device. *Nano Lett.* **2021**, *21* (13), 5671−5680.
(28) Maeki, M.; Uno, S.; Niwa, A.; Okada, Y.; Tokeshi, M. Microfluidic Technologies and Devices for Lipid Nanoparticle-Based RNA Delivery. *J. Controlled Release* **2022**, *344*, 80−96.
(29) Parasassi, T.; De Stasio, G.; d'Ubaldo, A.; Gratton, E. Phase Fluctuation in Phospholipid Membranes Revealed by Laurdan Fluorescence. *Biophys. J.* **1990**, *57* (6), 1179−1186.
(30) Parasassi, T.; Gratton, E.; Yu, W. M.; Wilson, P.; Levi, M. Two-Photon Fluorescence Microscopy of Laurdan Generalized Polarization Domains in Model and Natural Membranes. *Biophys. J.* **1997**, *72* (6), 2413−2429.
(31) Owen, D. M.; Rentero, C.; Magenau, A.; Abu-Siniyeh, A.; Gaus, K. Quantitative Imaging of Membrane Lipid Order in Cells and Organisms. *Nat. Protoc.* **2012**, *7* (1), 24−35.
(32) Wilson, S. C.; Baryza, J. L.; Reynolds, A. J.; Bowman, K.; Keegan, M. E.; Standley, S. M.; Gardner, N. P.; Parmar, P.; Agir, V. O.; Yadav, S.; Zunic, A.; Vargeese, C.; Lee, C. C.; Rajan, S. Real Time Measurement of PEG Shedding from Lipid Nanoparticles in Serum via NMR Spectroscopy. *Mol. Pharm.* **2015**, *12* (2), 386−392.
(33) Walderhaug, H.; Söderman, O.; Topgaard, D. Self-Diffusion in Polymer Systems Studied by Magnetic Field-Gradient Spin-Echo NMR Methods. *Prog. Nucl. Magn. Reson. Spectrosc.* **2010**, *56* (4), 406−425.
(34) Hama, S.; Itakura, S.; Nakai, M.; Nakayama, K.; Morimoto, S.; Suzuki, S.; Kogure, K. Overcoming the Polyethylene Glycol Dilemma via Pathological Environment-Sensitive Change of the Surface Property of Nanoparticles for Cellular Entry. *J. Controlled Release* **2015**, *206*, 67−74.
(35) Guo, X.; Liu, F.; Deng, J.; Dai, P.; Qin, Y.; Li, Z.; Wang, B.; Fan, A.; Wang, Z.; Zhao, Y. Electron-Accepting Micelles Deplete Reduced Nicotinamide Adenine Dinucleotide Phosphate and Impair Two Antioxidant Cascades for Ferroptosis-Induced Tumor Eradication. *ACS Nano* **2020**, *14* (11), 14715−14730.
(36) Vercauteren, D.; Vandenbroucke, R. E.; Jones, A. T.; Rejman, J.; Demeester, J.; De Smedt, S. C.; Sanders, N. N.; Braeckmans, K. The Use of Inhibitors to Study Endocytic Pathways of Gene Carriers: Optimization and Pitfalls. *Mol. Ther.* **2010**, *18* (3), 561−569.
(37) Plazzo, A. P.; Höfer, C. T.; Jicsinszky, L.; Fenyvesi, É.; Szente, L.; Schiller, J.; Herrmann, A.; Müller, P. Uptake of a Fluorescent Methyl-β-Cyclodextrin via Clathrin-Dependent Endocytosis. *Chem. Phys. Lipids* **2012**, *165* (5), 505−511.
(38) Lu, D.; An, Y.; Feng, S.; Li, X.; Fan, A.; Wang, Z.; Zhao, Y. Imidazole-Bearing Polymeric Micelles for Enhanced Cellular Uptake, Rapid Endosomal Escape, and On-Demand Cargo Release. *AAPS PharmSciTech* **2018**, *19* (6), 2610−2619.
(39) Adler, J.; Parmryd, I. Colocalization Analysis in Fluorescence Microscopy. *Methods Mol. Biol.* **2012**, *931*, 97−109.
(40) Chen, J.; Chen, J.; Xu, Q. Current Developments and Challenges of MRNA Vaccines. *Annu. Rev. Biomed. Eng.* **2022**, *24*, 85−109.
(41) Li, S.-D.; Huang, L. Pharmacokinetics and Biodistribution of Nanoparticles. *Mol. Pharm.* **2008**, *5* (4), 496−504.
(42) Teramo, K. A.; Klemetti, M. M.; Widness, J. A. Robust Increases in Erythropoietin Production by the Hypoxic Fetus is a Response to Protect the Brain and Other Vital Organs. *Pediatr. Res.* **2018**, *84* (6), 807−812.
(43) Cabral, H.; Li, J.; Miyata, K.; Kataoka, K. Controlling the Biodistribution and Clearance of Nanomedicines. *Nat. Rev. Bioeng.* **2024**, *2* (3), 214−232.
(44) Van Duyne, G. D. Cre Recombinase. In *Mobile DNA III*; Wiley, 2015; pp 119−138.
(45) Liu, Y.; Wang, J.; Xiong, Q.; Hornburg, D.; Tao, W.; Farokhzad, O. C. Nano-Bio Interactions in Cancer: From Therapeutics Delivery to Early Detection. *Acc. Chem. Res.* **2021**, *54* (2), 291−301.
(46) Marques, C.; Hajipour, M. J.; Marets, C.; Oudot, A.; Safavi-Sohi, R.; Guillemin, M.; Borchard, G.; Jordan, O.; Saviot, L.; Maurizi, L. Identification of the Proteins Determining the Blood Circulation Time of Nanoparticles. *ACS Nano* **2023**, *17* (13), 12458−12470.
(47) Kumar, A. R. K.; Shou, Y.; Chan, B.; L, K.; Tay, A. Materials for Improving Immune Cell Transfection. *Adv. Mater.* **2021**, *33* (21), No. e2007421.
(48) Yue, Y.; Jin, F.; Deng, R.; Cai, J.; Dai, Z.; Lin, M. C.; Kung, H. F.; Mattebjerg, M. A.; Andresen, T. L.; Wu, C. Revisit Complexation between DNA and Polyethylenimine-Effect of Length of Free Polycationic Chains on Gene Transfection. *J. Controlled Release* **2011**, *152* (1), 143−151.
(49) Ju, Y.; Lee, W. S.; Pilkington, E. H.; et al. Anti-PEG Antibodies Boosted in Humans by SARS-CoV-2 Lipid Nanoparticle mRNA Vaccine. *ACS Nano* **2022**, *16* (8), 11769−11780.
(50) Suzuki, T.; Suzuki, Y.; Hihara, T.; et al. PEG Shedding-Rate-Dependent Blood Clearance of PEGylated Lipid Nanoparticles in Mice: Faster PEG Shedding Attenuates Anti-PEG IgM Production. *Int. J. Pharmaceut.* **2020**, *588*, 119792.
(51) Maeki, M.; Kimura, N.; Sato, Y.; Harashima, H.; Tokeshi, M. Advances in Microfluidics for Lipid Nanoparticles and Extracellular Vesicles and Applications in Drug Delivery Systems. *Adv. Drug Delivery Rev.* **2018**, *128*, 84−100.
(52) Juang, V.; Chang, C.-H.; Wang, C.-S.; Wang, H.-E.; Lo, Y.-L. pH-Responsive PEG-Shedding and Targeting Peptide-Modified Nanoparticles for Dual-Delivery of Irinotecan and MicroRNA to Enhance Tumor-Specific Therapy. *Small* **2019**, *15* (49), No. e1903296.


https://doi.org/10.1021/acsnano.4c09399
*ACS Nano* XXXX, XXX, XXX−XXX